# Electron Density of Semi-Bridging Carbonyls. Metamorphosis of CO Ligands Observed *via* Experimental and Theoretical Investigations on [FeCo(CO)$_8$]$^-$

Piero Macchi,*,†,‡ Luigi Garlaschelli,§ and Angelo Sironi*,†,‡

*Contribution from the Dipartimento di Chimica Strutturale e Stereochimica Inorganica, Università di Milano, via Venezian 21, 20133 Milano, Italy, CNR−ISTM, via Golgi 19, 20133 Milano, and Dipartimento di Chimica Inorganica Metallorganica e Analitica, Università di Milano, Via Venezian 21, 20133 Milano, Italy.*

***Abstract:*** The electron density distribution in a transition-metal dimer containing a semibridging carbonyl is determined through experimental X-ray diffraction and quantum chemical computations. The changes occurring during the evolution from terminal to bridging coordinations are described by a "structure-correlation-like" approach and by a theoretical investigation along the conversion path. The smooth continuum of conformations observed in the solid state is explained in terms of the mutual interplay of direct M−M and M−CO and indirect M- - -M and M- - -C interactions, which can be characterized by interatomic delocalization indexes, within the framework of Quantum Theory of Atoms in Molecules.

## Introduction

A metal−metal bond in a di- or polynuclear complex tends to be its most characteristic structural feature and at the same time bears a reactive potential that sets it apart from the other component of the molecule.[1] However, despite the huge amount of synthetic, structural, spectroscopic, and theoretical "observations" on metal−metal interactions their nature is still a matter of debate. Indeed, questions about the actual presence of the metal−metal bond itself have been raised since the crystal structure determination (hence, the discovery) of the earlier dimeric metal carbonyls, namely [Fe$_2$(CO)$_9$][2] and [Mn$_2$(CO)$_{10}$].[3] The answer is not as straightforward as that usually given in the textbooks that apply the 18-electrons rule; indeed, it is always difficult (and often ambiguous) to work backward from a physical observation to the nature of the bonding.[4]

The presence of bridging carbonyls ($\mu_2$−CO) increases the complexity of the problem because the occurrence of a direct metal−metal bond can now be even more questioned.[5] However, the easy mobility about the metal skeleton (fluxionality) of the

carbonyls in solution and the smooth continuum encompassing terminal, bent semi-bridging and symmetrically bridging CO groups in the solid state are well-known.[6] For this reason, it is challenging to understand the subtle interplay between M−C and M−M interactions along the terminal-CO$\leftrightarrow\mu_2$−CO conversion path.

The analysis of the geometries of dimeric and polinuclear species present in the Cambridge Structural Database (CSD)[7] shows that there is no substantial discontinuity between terminal (**I**) and symmetrical bridging (**III**) coordination modes (see Figure 1).[8] Conformations **I** and **III** are reasonably well-defined, but a clear breakdown between the different bonding modes is not possible. We address as conformation **II** the central region that we tentatively confine in the 2.0−3.0 Å M···C distance range (for first transition metal dimers).

Many theoretical "observations" support the hypothesis that **I** has a single, localized 2-center-2-electron (2c-2e) M−M bond,[9] whereas **III** is often depicted as a delocalized system where the metal−metal interaction is mainly mediated[10] by the bridging CO with some residual (and controversial) direct contribution.[11] Doubts about the presence of a M−M bond in [Mn$_2$(CO)$_{10}$] came from early analyses of experimental[12] or theoretical[13] deformation densities, which could not find significant ac-

---

* To whom correspondence should be addressed. E-mail: piero@ csmtbo.mi.cnr.it; angelo@csmtbo.mi.cnr.it.
† Dipartimento di Chimica Strutturale e Stereochimica Inorganica, Università di Milano.
‡ CNR−ISTM.
§ Dipartimento di Chimica Inorganica Metallorganica e Analitica, Università di Milano.

(1) Gade, L. H. *Angew. Chem., Int. Ed.* **2000**, *39*, 2658−2678, and references therein.
(2) Powell, M. H.; Ewens, R. V. G. *J. Chem. Soc.* **1939**, 286−292.
(3) Dahl, L. F.; Rundle, R. E. *Acta Crystallogr.* **1963**, *16*, 419−426.
(4) Noteworthy, also the covalent/electrostatic nature of the M−CO interaction in mononuclear complexes is still a matter of discussion; see Frenking, G.; Fröhlich, N.*Chem. Rev.* **2000**, *100*, 717−774, and references therein.
(5) Bauschlicher, C. W. *J. Chem. Phys.* **1986**, *84*, 872−875.

(6) Sironi, A. *Metal Clusters in Chemistry*; Braunstein, Oro, Raithby, Eds.; Wiley-VCH: New York, 1999; Vol. 2, 937−959, and references therein.
(7) Cambridge Crystallographic Data Centre, June 2001.
(8) A similar picture has been previously reported by Orpen, A. G. *Chem. Soc. Rev.* **1993**, *22*, 191−197.
(9) Heijser, W.; Baerends, E. J.; Ros, P. *Faraday Symp.* **1980**, *14*, 211−234.
(10) (a) Bauschlicher, C. W. *J. Chem. Phys.* **1986**, *84*, 872−875. (b) Summerville, R. H.; Hoffmann, R. *J. Am. Chem. Soc.* **1979**, *101*, 3821−3831.
(11) Mealli, C.; Proserpio, D. M. *J. Organomet. Chem.* **1990**, *386*, 203−208.
(12) Martin, M.; Rees, B.; Mitschler, A. *Acta Crystallogr.* **1982**, *B38*, 6−15.
(13) Hall, M. B. In *Electron Distribution and the Chemical Bond*; Coppens, P., Hall, M. B., Eds.; Plenum Press: New York, 1982; p 205.
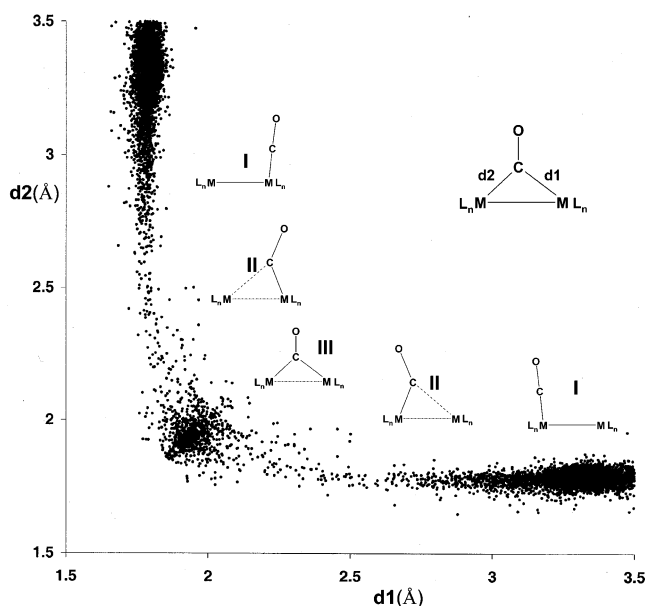
---

**Figure 1.** Correlation plot for the moiety M(CO)M (M = Fe, Co, Ni); each fragment retrieved from the CSD[7] contributes to two (symmetrically related) points in the configurational space.

cumulation of electron density inside the metal−metal bonding region. In addition, some very early calculations[14] addressed the direct Mn⋯CO long-range interactions as the predominant source of stability. It was only after the introduction of "chemically oriented" promolecules that deformation densities could reveal some, at least small, covalent M−M bonding contribution.[13] Eventually, the quantum theory of atoms in molecules (QTAM)[15] approach revealed more consistently the presence of a direct M−M interaction in **I**[16,17] and supported the hypothesis of delocalized bonding in **III** (where a M−M bond path is absent[18,19]).

According to the structure correlation method,[20] Figure 1 is a representation of the terminal-to-bridging CO reaction path, i.e., a track of the elementary mechanism associated to most fluxional processes of metal carbonyl clusters. The aim of this work is to provide a description of such an elementary process by considering the evolution of the electron density (and its derived quantities) along the terminal-to-bridging CO coordinate. While it is possible to follow the "same" molecule along a given conformational rearrangement with theoretical computations, the structure correlation principle resorts to the concept of fragment in order to observe the "same" moiety in different but stable environments. Accordingly, here we will both compute the evolution of the electron density of [FeCo(CO)$_8$]$^-$ along a hypothetical terminal-to-bridging CO conversion path and merge (in a correlation like plot) our previous experimental results on [Co$_2$(CO)$_6$(AsPh$_3$)$_2$][16] and [Co$_4$(CO)$_{11}$(PPh$_3$)][18] (representative

of conformation **I** and **III**, respectively) with the new accurate electron density determination of [FeCo(CO)$_8$] [N(PPh$_3$)$_2$]. Having a semibridging carbonyl, the [FeCo(CO)$_8$]$^-$ anion is representative of the unsymmetrical coordination **II**.

## Experimental Section

**X-ray Data Collections.** The original crystal structure determination of [FeCo(CO)$_8$][N(PPh$_3$)$_2$] was significantly affected by crystal decay, which limited the resolution of the acquired data.[21] Thanks to the rapidity of the modern area-detectors, we could collect a more extensive preliminary room temperature (RT) dataset.[22] This experiment confirmed the lability of the crystals, whose decay was about 7% in 1 day. Nevertheless, the quality of the data collection was acceptable and allowed to refine quite accurately a RT geometry of the anion.

For the low-temperature experiment, a fresh crystal (0.34 × 0.26 × 0.1 mm) was screened, mounted on the goniometer head, and immediately put under a moderately cold (about −30 °C) nitrogen stream, to prevent any crystal damaging. Afterward, the crystal was slowly cooled to −150 °C, and the data collection started. The detector was positioned in three different $\theta$ settings (0°, 40°, 60°) with a detector−sample distance of 2.90(1) cm. The scan axes were either $\omega$ and $\phi$, with scan width of 0.3°. Eight runs were carried out with an acquisition time/frame of 20, 40, and 80 s for the three different $\theta$ settings, respectively. A total of 102 256 intensities were collected, 648 of which were discarded because they were partially obscured by the beam stop or the beam stop arm. The program SADABS[23] was used to correct for diffraction anisotropies and 123 intensities were rejected because they were judged outliers. The 101 485 good measures were then corrected for the $\theta$ dependent spherical absorption and merged[24] to 32 676 unique reflections. Note that the redundancy of low order data (those most important for determining the parameters of the correction) was about 9, whereas, including the high-order data as well, it is reduced to about 3, as it is always difficult carrying multiple measurements at high diffraction angles if the system is *triclinic* and the diffractometer is a three circle goniometer.

No intensity decay was observed at the end of the 4 day data collection.

A preliminary spherical atom refinement[25] was carried out starting from the room-temperature geometry. In their original paper,[21] Bau and co-workers located Co and Fe atoms based on stereochemical considerations, which favor the Co−C⋯Fe conformer over the Fe−C⋯Co one. The quality of those X-ray data did not allow further speculations. To confirm the correctness of that assignment, we can add the following arguments: (a) refinements of the low-temperature data afforded better agreement indexes[26] and smaller differences between the $U_{eq}$ factors of Co and Fe[27] for the Co−C⋯Fe conformation; (b) after exploring, with quantum mechanical methods, the gas-phase potential energy surface of [FeCo(CO)$_8$]$^-$ a true minimum ($C_s$ symmetry) is located only for the Co−C⋯Fe semibridging isomer; and (c) the residual map, after the multipolar refinement, is flat (see Supporting Information).

(14) Brown, D. A.; Chambers, W. J.; Fitzpatrick, N. J.; Rawilson, R. M. *J. Chem. Soc. A* **1971**, 720−725.

(15) Bader, R. F. W. *Atoms in Molecules. A Quantum Theory*; Cambridge University Press: Oxford U.K., 1991.

(16) Macchi, P.; Proserpio, D. M.; Sironi, A. *J. Am. Chem. Soc.* **1998**, *120*, 13 429−13 435.

(17) Bianchi, R.; Gervasio, G.; Marabello, D. *Chemm. Commun.* **1998**, 1535−1536.

(18) Macchi, P.; Garlaschelli, L.; Martinengo, S.; Sironi, A. *J. Am. Chem. Soc.* **1999**, *121*, 10 428−10 429.

(19) (a) Low, A. A.; Kunze, K. L.; MacDougall, P. J.; Hall, M. B. *Inorg. Chem.* **1991**, *30*, 1079−1086. (b) Bo, C.; Sarasa, J. P.; Poblet, J. M. *J Phys. Chem.* **1993**, *97*, 6362−6366.

(20) Bürgi, H.-B. *Angew. Chem.* **1975**, *87*, 461−475.

(21) Chin, H. B.; Smith, M. B.; Wilson, R. D.; Bau, R. *J. Am. Chem. Soc.* **1974**, *96*, 5285−5287.

(22) A crystal was mounted on a SMART-CCD diffractometer and three sets of 600 frames each were collected (30s/frame) in three different $\phi$ positions with $\omega$ scanning. A spherical atom model was refined against these data ($R_1$ = 0.0491; w$R_2$ = 0.1167). Atomic coordinates and principal distances and angles are included in the Supporting Information.

(23) Sheldrick, G. M. 1996 *SADABS*, University of Göttingen, Germany, unpublished.

(24) Farrugia, L. J. *J. Appl. Crystallogr.* **1999**, *32*, 837−838.

(25) Sheldrick, G. M. SHELX-97: *A Program for Structure Refinement*. University of Gottingen, Germany.

(26) For $I > 2\sigma(I)$: $R_1$ = 0.0372 vs 0.0485; w$R_2$ = 0.0899 vs 0.1106; for all data: $R_1$ = 0.0545 vs 0.0663; w$R_2$ = 0.0972 vs 0.1200. Even a high-order refinement (sin $\theta/\lambda > 0.7$ Å$^{-1}$) confirms the assignment. For $I > 2\sigma(I)$: $R_1$ = 0.0418 vs 0.0432; w$R_2$ = 0.0680 vs 0.0717; for all data: $R_1$ = 0.0741 vs 0.0756; w$R_2$ = 0.0787 vs. 0.0825.

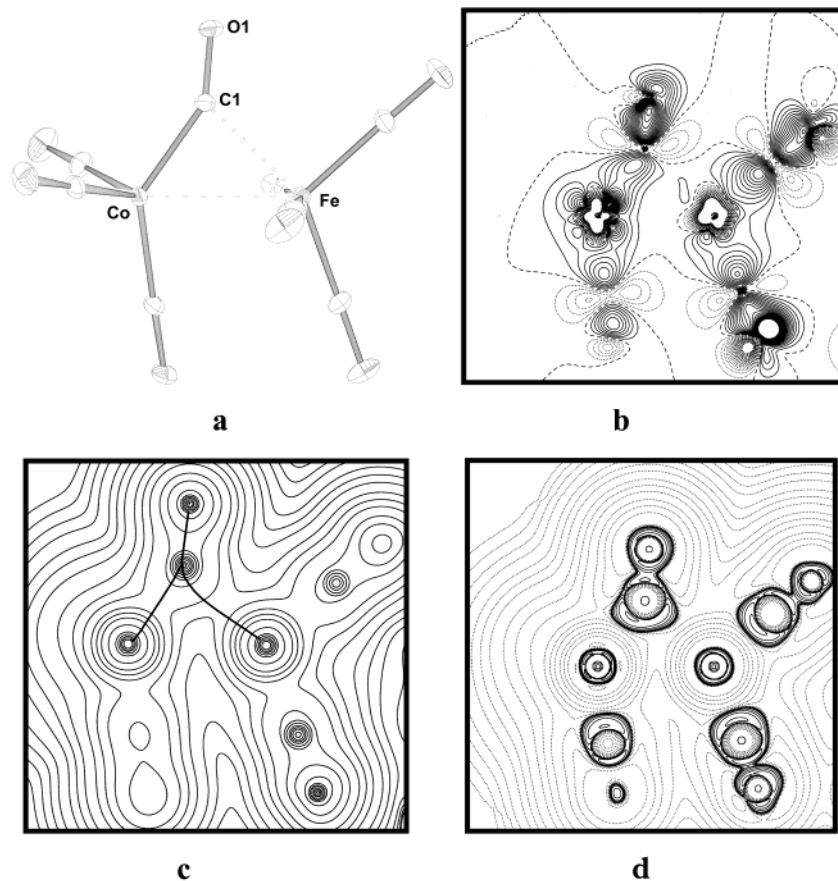(27) 5.3% vs. 26.9% (note that Co always has the largest $U_{eq}$).

**Figure 2.** (a) ORTEP representation of $[FeCo(CO)_8]^-$ anion with ellipsoids drawn at 50% probability level. (b) The static deformation density in the Fe−Co−C(1) plane; contours are drawn at $\pm 0.05$ e$\text{Å}^{-3}$, solid contours are positive values, dotted contours are negative; the dashed line corresponds to $\Delta\rho(r) = 0.0$. (c) Total electron density distribution in the same plane (contours drawn with exponential growth); Co−C(1), Fe−C(1), and C(1)−O(1) bond paths are superimposed. (d) $\nabla^2\rho(r)$ distribution in the same plane (negative contours are solid lines, with exponential growth; positive contours are dotted lines).

A modified version[28] of the XD code[29] was used for the multipolar refinements, using the Hansen and Coppens pseudo-atomic expansion[30]

$$\rho(\mathbf{r}) = \sum_{i=1}^{N} \rho_i(\mathbf{r} - \mathbf{r}_i)$$

$$\rho_i(\mathbf{r}_i) = P_{ic}\rho_{\text{core}}(\mathbf{r}_i) + \kappa^3\rho_{\text{valence}}(\kappa\mathbf{r}_i)P_{iv} +$$
$$\sum_{l=0}^{4}[\kappa'^3 R_l(\kappa\mathbf{r}_i)\sum_{m=0}^{l}P_{ilm\pm}y_{lm\pm}(\mathbf{r}_i/r_i)]$$

Relativistic atomic wave functions[31] were adopted for describing core and spherical valence. Co and Fe were expanded up to hexadecapole level; C, N, P, and O atoms up to octupole level; H atoms up to dipole level (with just one dipole oriented along the C−H direction). Positions and isotropic thermal parameters of hydrogens were fixed after a refinement using scattering factors polarized along the C−H bond[32] ($<d_{\text{C−H}}> = 1.05(2)$ Å). The radial part of the deformation density was constructed from single-$\zeta$ Slater type orbitals[33] for C, N, O (with $n_l =$

2,2,2,3), H ($n_l = 0,1$), and P ($n_l = 4,4,6,8$), and from 3d orbitals for the metals.[31] $\kappa$ and $\kappa'$ radial scaling parameters were refined for each 'chemically' independent atom (one Co, one Fe, one O, two C, one N; one P and one H). For oxygens, $\kappa'$ was fixed equal to $\kappa$ to avoid unrealistic expansions.[34] A similar procedure was necessary for phosphorus and nitrogen to avoid some correlation between the parameters of these two atoms. For Co and Fe, $\kappa$ and $\kappa'$ were constrained to be equal, given that the same radial functions are used for spherical valence monopole and higher multipoles. The 4s populations of both metals were tentatively refined, but their values always slightly exceeded 2.0. Therefore, they were constrained to 2.0. It is notable that this feature is almost reproducible in many low oxidation state complexes or clusters and confirmed by the populations of diffuse orbitals computed from theoretical calculations. Noteworthy, the population of ns electrons does not interfere with the $(n − 1)d$ refinement, because the two orbitals, although very close in energy, occupy completely different spatial regions (both in the real and the reciprocal space). To reduce the number of variables, hydrogen atoms were constrained to have the same populations. The quantity minimized was $\epsilon = \sum w(F_o^2 − F_c^2)^2$ based on the 25 332 reflections with $I > 2\sigma(I)$; weights were always taken as $w = 1/\sigma^2(F^2)$. Convergence was assumed when $|\delta\mathbf{x}|/\sigma(\mathbf{x}) < 0.01$ for each variable $\mathbf{x}$. No significant extinction was found. The largest residual feature (using all data) is 0.3 e/$\text{Å}^3$. A residual density map in the plane Fe−Co−C(1) is reported in the Supporting Information. A picture of the anion geometry is reported in Figure 2a. Crystallographic data and further details of the multipolar refinements are listed in Table 1.

(28) P. Macchi, 2000, unpublished results.
(29) Koritsanszky, T.; Howard, S. T.; Su, Z.; Mallinson, P. R.; Richter, T.; Hansen, N. K. *XD, Computer Program Package for Multipole refinement and Analysis of Electron Densities from Diffraction Data*, Free University of Berlin, Germany, June 1997.
(30) Hansen, N. K.; Coppens, P. *Acta Crystallogr. Sect. A* **1978**, *34*, 909−921.
(31) (a) Su, Z.; Coppens, P. *Acta Crystallogr.* **1998**, *A54*, 646−652. (b) Macchi, P.; Coppens, P. *Acta Crystallogr.* **2001**, *A57*, 656−662.
(32) Stewart, R. F.; Bentley, J.; Goodman, B. *J. Chem. Phys.* **1975**, *63*, 3786−3793.
(33) Clementi, E.; Raimondi, D. L. *J. Chem. Phys.* **1963**, *38*, 2686−2689. For sp shell, the exponents of 2s and 2p orbitals are simply averaged.
(34) Abramov, Y.; Volkov, A.; Coppens, P. *Chem. Phys. Lett.* **1999**, *311*, 81−86.

**Table 1.** Crystallographic Data of [FeCo(CO)$_8$][N(PPh$_3$)$_2$], Summary of Data Collection and Residual Indexes after Multipolar Refinement

| compd | [FeCo(CO)$_8$] [N(PPh$_3$)$_2$] |
|---|---|
| instrument | SMART CCD |
| $T$ (K) | 125(2) K |
| $a$ (Å) | 10.562(1) |
| $b$ (Å) | 12.545(1) |
| $c$ (Å) | 15.190(1) |
| $\alpha$ (°) | 95.85(1) |
| $\beta$ (°) | 91.99(2) |
| $\gamma$ (°) | 97.57(1) |
| $V$ (Å$^3$) | 1982.4 |
| $\lambda$ (Å) | 0.7107 |
| $max \sin(\theta)/\lambda$ (Å$^{-1}$) | 1.06 |
| space group | P-1 |
| intensities collected | 102 256 |
| unique reflections | 32 676 |
| $R_{int}$ | 0.023 |
| $R_\sigma$ | 0.032 |
| Included in the refinement ($I > 2\sigma(I)$) | 25 332 |
| residuals after multipolar refinement | |
| $R_1$ ($I > 2\sigma(I)$) | 0.0275 |
| $R_1$ (all reflections) | 0.0450 |
| $R_2$ ($I > 2\sigma(I)$) | 0.0272 |
| $R_2$ (all reflections) | 0.0300 |
| w$R_1$ | 0.0198 |
| w$R_2$ | 0.0361 |
| gof | 1.27 |

In this paper, the electron density of the [N(PPh$_3$)$_2$]$^+$ cation is not discussed, but we can simply mention that analyses of thermal parameters (rigid body test), deformation maps and topological indexes give results in agreement with expectation, confirming the good quality of the experiment.

**Theoretical Calculations.** All computations were performed using GAUSSIAN98.[35] The [M$_2$(CO)$_8$]$^{n-}$ molecules reported in Table 4 were optimized using the B3LYP[36] hybrid functional and two kinds of basis sets: (1) relativistic small-core effective core potentials[37] with a basis set splitting (341/311/41) for the metals and double-$\zeta$ quality[38] all-electron basis (721/41) for C and O (hereafter, this basis set is called *ecp1*), with two polarization *d* functions on C and O (basis set *ecp2*) and one *f* function on the metals (basis set *ecp3*); (2) all electron basis set of 6-311++G quality for both the second row elements and the metals (*ae1*), including one polarization *d* function for second row atoms and one *f* function for the metals (*ae2*). Calculations on prototype molecules, reported in Table 3, were performed with basis sets *ae2* and QCISD method (in a few addressed exceptions, the geometry was optimized at the B3LYP level). Topological properties of the SCF and QCISD electron densities were investigated with the programs AIM-PAC,[39] AIM2000,[40] MORPHY98,[41] and WBADER.[42] Mayer bond orders were computed with the software MAYER.[43]

**Structural Correlation Analysis.** Crystal structure analyses were performed using the Cambridge Structural Database (CSD).[7] The crystallographic data were screened according to the following criteria: (a) agreement index $R1 < 0.100$; (b) no disorder in the fragment under study; (c) no unresolved errors; and (d) perfect match between chemical and crystal connectivity.

**[FeCo(CO)$_8$]$^-$ Experimental vs Theoretical Geometries.** The structure of the [FeCo(CO)$_8$]$^-$ anion is highlighted in Figure 2a. Due to the overall symmetry of the crystal packing (which lacks of crystallographic mirrors) the anion in the solid state is slightly distorted from the idealized $C_s$ symmetry of the gas phase. A collection of the pertinent bond lengths observed at 125 K and computed for the gas-phase anions is reported in Table 2.

In the optimized geometry (at B3LYP/*ae2* level), the terminal carbonyls have, on average, $d_{Co-C} = 1.79$ Å, $d_{Fe-C} = 1.80$ Å, and $d_{C-O} = 1.15$ Å, whereas the semibridging carbonyl has significantly larger Co–C (1.83 Å) and C–O (1.17 Å) distances. In neutral cobalt complexes, terminal carbonyls have Co–C distances in the range 1.80–1.82 Å, whereas in anionic systems, like [Co(CO)$_4$]$^-$,[44] they significantly shorten (down to 1.76 Å) with C–O elongation (from 1.14 to 1.16 Å) due to the larger back-donation. A similar trend is observed for iron ($d_{Fe-C} = 1.82$ Å in neutral and 1.77 Å in anionic derivatives).[44] In [FeCo(CO)$_8$]$^-$, the M–C bond distances are intermediate between those of (pertinent) neutral and anionic species, this suggests that the charge is almost equally delocalized over the two parts of the molecule.

Compared to the corresponding terminal CO groups, symmetric bridges (in neutral or anionic dimers) have C–O distances elongated by at least 0.02 Å, see for example Table 4. Thus, despite its strong asymmetry, the semibridging carbonyl here reported is as perturbed as a symmetrically bridging group, showing that the effects of a bi-coordination have almost entirely occurred.

The experimental and theoretical geometries are in quite close agreement, but for Fe–Co and Fe–C(1) distances, which are significantly shorter in the solid-state geometry (2.6120(2) Å vs 2.700 and 2.1544(6) Å vs 2.251 Å, respectively). A longer metal–metal distance in the gas-phase is quite common for unsupported dimers,[45] and similar observations are reported for weak metal–ligand bindings,[46] as it could be classified in the interaction of Fe with the semibridging carbonyl. On the other hand, the hyperbolic shape of the terminal-to-bridge conversion path (Figure 1) explains the negligible difference observed for the Co–C(1) distance. Gas-phase optimizations with other basis sets confirm the disagreement with even longer semibridging distance (for example, at B3LYP/*ecp3* level Fe–Co = 2.677 Å; Fe–C(1) = 2.297 Å; Co–C(1) = 1.808 Å). Quite interestingly, at room-temperature Fe–C(1) is also larger (2.239(4) Å),[47] in agreement with the original room-temperature experiment by Bau and co-workers.[21] Thus, the crystal packing (more

(35) Frisch, M. J.; Trucks, G. W.; Schlegel, H. B.; Scuseria, G. E.; Robb, M. A.; Cheeseman, J. R.; Zakrzewski, V. G.; Montgomery, J. A., Jr.; Stratmann, R. E.; Burant, J. C.; Dapprich, S.; Millam, J. M.; Daniels, A. D.; Kudin, K. N.; Strain, M. C.; Farkas, O.; Tomasi, J.; Barone, V.; Cossi, M.; Cammi, R.; Mennucci, B.; Pomelli, C.; Adamo, C.; Clifford, S.; Ochterski, J.; Petersson, G. A.; Ayala, P. Y.; Cui, Q.; Morokuma, K.; Malick, D. K.; Rabuck, A. D.; Raghavachari, K.; Foresman, J. B.; Cioslowski, J.; Ortiz, J. V.; Stefanov, B. B.; Liu, G.; Liashenko, A.; Piskorz, P.; Komaromi, I.; Gomperts, R.; Martin, R. L.; Fox, D. J.; Keith, T.; Al-Laham, M. A.; Peng, C. Y.; Nanayakkara, A.; Gonzalez, C.; Challacombe, M.; Gill, P. M. W.; Johnson, B. G.; Chen, W.; Wong, M. W.; Andres, J. L.; Head-Gordon, M.; Replogle, E. S.; Pople, J. A. *Gaussian 98*; Gaussian, Inc.: Pittsburgh, PA, 1998.
(36) Becke, A. D. *J. Chem. Phys.* **1993**, *98*, 5648.
(37) Hay, P. J.; Wadt, W. R. *J. Chem. Phys.* **1985**, *82*, 299.
(38) Dunning, T. H.; Hay, P. J. *Modern Theoretical Chemistry*; Schaefer, H. F., III, Ed.; Plenum: New York, 1976, *3*, 1.
(39) Biegler-König, F. W.; Bader, R. F. W.; Ting-Hua, T. *J. Comput. Chem.* **1982**, *3*, 317−328.
(40) Biegler-König, F. W. AIM2000, version 1.0, University of Applied Sciences, Bielefeld, Germany.

(41) Popelier, P. L. A. *Comput. Phys. Commun.* **1996**, *93*, 212−240; Popelier, P. L. A. *Chem. Phys.* **1994**, *228*, 160−164.
(42) Girones, X.; Ponec, R.; Roithova, J. Program WBader, version 1.0, **2001**.
(43) Bridgeman, A. J.; Cavigliasso, G.; Ireland, L. R.; Rothery, J. *J. Chem. Soc.*, *Dalton Trans.* **2001**, 2095−2108.
(44) Macchi, P.; Sironi, A., *Coord. Chem. Rev.*, in press.
(45) Rosa, A.; Ehlers, A. W.; Baerends, E. J.; Snijders, J. G.; te Velde, G. *J. Phys. Chem.* **1996**, *100*, 5690−5696.
(46) Jonas, V.; Frenking, G.; Reetz, M. T. *J. Am. Chem. Soc.* **1994**, *116*, 8741−8753.
(47) However, there is no substantial difference in the Fe–Co distance.

***Table 2.*** Summary of the QTAM Analysis for the Main Interactions in $[FeCo(CO)_8]^-$ from the Experimental Multipolar Density and the B3LYP/*ae2* Optimization

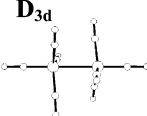| bond | | $d$ Å | $d1$ Å | $d2$ Å | $\rho(r)$ e Å$^{-3}$ | $\nabla^2\rho(r)$ e Å$^{-5}$ | $G(r)/\rho(r)$ h e$^{-1}$ | $H(r)/\rho(r)$ h e$^{-1}$ |
|---|---|---|---|---|---|---|---|---|
| Fe−C(1) | expt | 2.1544(6) | 1.098 | 1.057 | 0.466(3) | 3.86(1) | 0.870 | −0.290 |
| | theor | 2.251 | 1.111 | 1.140 | 0.42 | 2.8 | 0.700 | −0.230 |
| Co−C(1) | expt | 1.8292(6) | 0.967 | 0.862 | 1.020(6) | 7.07(2) | 1.138 | −0.653 |
| | theor | 1.828 | 0.942 | 0.887 | 0.95 | 8.4 | 1.012 | −0.392 |
| < Co−C > | expt | 1.78(1) | 0.933(7) | 0.85(1) | 1.08(5) | 10.0(1) | 1.278(8) | −0.63(4) |
| | theor | 1.79(1) | 0.917(1) | 0.87(1) | 0.98(3) | 13.4(5) | 1.33(2) | −0.38(1) |
| < Fe−C > | expt | 1.80(1) | 0.93(1) | 0.87(2) | 1.06(7) | 11.0(5) | 1.32(2) | −0.59(5) |
| | theor | 1.80(2) | 0.914(7) | 0.88(2) | 0.98(5) | 12.6(2) | 1.30(1) | −0.40(3) |
| C(1)−O(1) | expt | 1.178(1) | 0.396 | 0.782 | 2.97(2) | 3.08(9) | 1.709 | −1.636 |
| | theor | 1.171 | 0.398 | 0.773 | 2.97 | 7.0 | 1.879 | −1.713 |
| < C−O > | expt | 1.154(3) | 0.388(5) | 0.766(5) | 3.05(10) | 17(9) | 1.9(1) | −1.6(1) |
| | theor | 1.153(2) | 0.393(1) | 0.760(1) | 3.10(1) | 9.6(2) | 1.95(1) | −1.737(4) |

Experimentally, $H(r)$ and $G(r)$ are computed according to the algorithm proposed by Abramov.[70] Number in parentheses are standard deviations from the mean, for all the parameters that were averaged. Standard uncertainties are reported for the experimentally derived parameters of Fe−C(1), Co−C(1), and C(1)−O(1) bonds.

***Table 3.*** Main Features of the Electron Density Distribution in Some Prototype Bonding Interactions (computed at QCISD/*ae2* Level)

| bond | $d_{A-cp}$ Å | $d_{B-cp}$ Å | $\rho(r_b)$ e Å$^{-3}$ | $\nabla^2\rho(r_b)$ eÅ$^{-5}$ | $H(r_b)/\rho$ he$^{-1}$ | $G(r_b)/\rho$ he$^{-1}$ | $\oint_{A\cap B}\rho$ eÅ$^{-1}$ | $\delta$ (**A**,**B**) [SCF] | Mayer BO |
|---|---|---|---|---|---|---|---|---|---|
| H−H | 0.372 | 0.372 | 1.750 | −24.71 | −1.028 | 0.040 | 1.42 | 1.00 | 1.00 |
| H$_3$C−CH$_3$* | 0.766 | 0.766 | 1.623 | −13.64 | −0.844 | 0.256 | 2.16 | 1.01 | 0.80 |
| H$_2$C=CH$_2$ | 0.670 | 0.670 | 2.262 | −23.83 | −1.159 | 0.421 | 2.94 | 1.90 | 1.96 |
| HC≡CH | 0.605 | 0.605 | 2.659 | −27.10 | −1.425 | 0.711 | 3.70 | 2.85 | 3.67 |
| H$_3$C−OCH$_3$* | 0.481 | 0.933 | 1.744 | −9.94 | −1.401 | 1.002 | 2.32 | 0.90 | 0.90 |
| H$_2$C=O | 0.412 | 0.799 | 2.755 | −1.40 | −1.680 | 1.644 | 3.03 | 1.58 | 2.16 |
| C≡O | 0.383 | 0.751 | 3.194 | 20.29 | −1.759 | 2.203 | 3.17 | 1.80 | 2.21 |
| Na−F | 0.923 | 1.063 | 0.292 | 8.63 | 0.288 | 1.785 | 0.46 | 0.27 | 0.33 |
| Ne−Ne | 1.577 | 1.577 | 0.012 | 0.36 | 0.593 | 1.514 | 0.02 | 0.002 | 0.01 |
| Na−Na | 1.582 | 1.582 | 0.055 | −0.06 | −0.160 | 0.080 | 0.50 | 1.00 | 1.00 |
| K−K | 1.990 | 1.990 | 0.032 | 0.03 | −0.071 | 0.14 | 0.42 | 0.82 | 0.99 |
| (CO)$_4$Co−Co(CO)$_4$* | 1.373 | 1.373 | 0.227 | 0.06 | −0.278 | 0.296 | 1.54 | 0.46 | 0.67 |

*Geometry optimization at B3LYP/*ae2* level

***Table 4.*** Collection of Pertinent Parameters of the Equilibrium $[M_2(CO)_8]^{q-}$ Isomers Optimized at B3LYP/*ecp2* Level

| Molecular Structure | Compound | energy (kcal/mol) | $d_{M-M}$ (Å) | $d_{(M-C)opp.}$ (Å) | $d_{(M-C)prox}$ (Å) | $d_{M\cdots Cprox}$ (Å) | $d_{(C-O)opp.}$ (Å) | $d_{(C-O)prox}$ (Å) | M-C-O prox (°) | Imag. Freq. |
|---|---|---|---|---|---|---|---|---|---|---|
| **D$_{3d}$** | Co$_2$(CO)$_8$ | 3.6 | 2.69 | 1.78 | 1.81 | 3.11* | 1.147 | 1.150 | 177.6 | 0 |
| | [FeCo(CO)$_8$]$^-$ | 3.0 | 2.82 | 1.74; 1.76 | 1.79; 1.78 | 3.07*; 3.28* | 1.164; 1.160 | 1.159;1.164 | 177.5; 175.5 | 0 |
| | [Fe$_2$(CO)$_8$]$^{2-}$ | 0.0 | 2.89 | 1.73 | 1.77 | 3.22* | 1.179 | 1.175 | 175.4 | 0 |
| **D$_{2d}$** | Co$_2$(CO)$_8$ | 0.0 | 2.64 | 1.80 | 1.79 | 2.85* | 1.148 | 1.151 | 175.1 | 0 |
| | [FeCo(CO)$_8$]$^-$ | 0.0 | 2.68* | 1.76; 1.76 | 1.79; 1.81 | 2.29; 3.01* | 1.162; 1.163 | 1.159; 1.176 | 178.8; 153.1 | 0 |
| | [Fe$_2$(CO)$_8$]$^{2-}$ | 1.2 | 2.78 | 1.74 | 1.78 | 2.92* | 1.180 | 1.174 | 174.0 | 0 |
| **C$_{2v}$** | Co$_2$(CO)$_8$ | 3.1 | 2.55* | 1.81 | 1.95 | 1.95 | 1.146 | 1.171 | 139.2 | 0 |
| | [FeCo(CO)$_8$]$^-$ | 4.0 | 2.59* | 1.78; 1.78 | 1.90; 2.07 | 2.07; 1.90 | 1.161; 1.160 | 1.181 | 147.2; 131.4 | 1 |
| | [Fe$_2$(CO)$_8$]$^{2-}$ | 5.9 | 2.64* | 1.73 | 1.98 | 1.98 | 1.179 | 1.195 | 138.2 | 1 |

*a* For each stereochemistry, we distinguish "opposed carbonyls" (which have M−M-C > 90°) and "proximal carbonyls" (which have M−M-C < 90°). For each compound the energy is related to the most stable isomer. In [FeCo(CO)$_8$]$^-$, the first entry refers to Fe−CO parameters, the second to Co−CO. A bond path characterises all the interactions but those labelled with *.

effective as the temperature is lowered) is responsible of a significant distortion in the semibridging conformation, pushing the anion somewhat closer to isomer **III** in the correlation plot of Figure 1. As we will see, this "compression" does not qualitatively affect the bonding mechanism of the system investigated. However, differences such as those here observed

may be quite common whenever dealing with transition metal complexes,[48] and they should be always taken into account, if properties of crystals are investigated with the aim of extracting some "universal" information.

(48) Martin, A.; Orpen, A. G. *J. Am. Chem. Soc.* **1996**, *118*, 1464−1470.

**Chart 1**
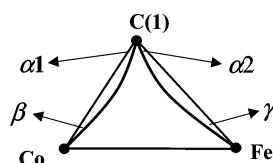


### Electron Density Distribution in [FeCo(CO)$_8$]$^-$

The static deformation density map[49] in the Fe−C(1)−Co plane (Figure 2b) shows no substantial density in the intermetallic region and a small accumulation along the Fe−C(1) direction. It is quite notable that most of the "donor" density surrounding C(1) is still directed toward the cobalt atom, though it is no longer associated to a "hole" in the metal 3*d* shell density, as it typically occurs for terminal carbonyls. The problematic use of deformation density for revealing M−M interactions is even more relevant when dealing with bridging or partially bridging ligands, that may be actually responsible for a reorientation of the metal orbitals and a quenching of the metal−metal bond. Thus, a straightforward interpretation of the deformation density in [FeCo(CO)$_8$]$^-$ is not possible in the absence of a more accurate QTAM investigation of the total electron density.

In this respect, the first important feature is the *molecular graph*, i.e., the topology of the bond paths (*bp*)[50] and their shape. Both in the experimental and in the gas-phase optimized geometry, the molecular graph lacks a direct metal−metal bond path (see Figures 2c and 3). At C(1), the Fe−C(1) and Co−C(1) bond paths are inwardly curved (inside the hypothetical Fe−C(1)−Co triangle) and the Co−C(1)−Fe bond path angle (*bpa*) is significantly smaller than the geometrical one (see Figure 2c and Chart 1). Experimentally, $\alpha_1 = 2.4°$ and $\alpha_2 = 7.3°$; theoretically, $\alpha_1 = 3.4°$ and $\alpha_2 = 12.3°$. Interestingly, the bond paths are inwardly curved also at the metal atoms (expt $\beta = 4.1°$; $\gamma = 4.0°$; theor $\beta = 5.4°$; $\gamma = 2.8°$). As it was noticed in other examples, and particularly in symmetrically bridged carbonyl systems,[18] this is reminiscent of a molecular orbital (MO) picture based on three-center delocalized bonding (even in the absence of one edge of the ring, here the M−M one). The asymmetry of the system is of course manifested by the electron densities of the M−C bond critical points (see Table 2).

Another interesting feature of the total electron density comes from the analysis of the shape of the Laplacian distribution ($\nabla^2\rho(r)$). A unique valence shell charge concentration (VSCC) is found around the semi-bridging carbonyl carbon (C(1)), see Figure 2d and 3. It is oriented toward Co, but the envelope of the carbonyl lone pair density is definitely larger than that of a terminal carbonyl.[51] The oxygen O(1) has instead three VSSCs, one pointing along the O−C bond and two nonbonded ones forming angles of ca. 130° (with good agreement between theory and experiment). Again, this is reminiscent of symmetrically bridged carbonyls[19b] and it is at variance from terminal carbonyls, whose oxygens have one bonded VSCC (directed

toward the carbon) and a single nonbonded VSCC (almost opposed to the carbon). Thus, many features of the Laplacian around the semibridging ligand have strong similarities with those of a bridging group, apart for the inherent asymmetry of the system.

**Bond Indexes for Characterizing Interactions with Transition Metals.** As demonstrated by Bader, the properties of the electron density evaluated at the *bcp* are fingerprints revealing the nature of the atomic interaction. Strong electron-sharing character is associated to large amount of electron density at the *bcp* and local concentration of the charge ($\nabla^2\rho(r_b) < 0$). Interactions between closed-shell atoms have instead opposite features. However, as discussed in a previous paper,[16] bonds involving heavy atoms have different Laplacian distributions, because their valence shell is normally "hidden" in the anomalous distribution of shell maxima and minima of the atomic $\nabla^2\rho(r)$ function. For these interactions, the shared or closed shell character is not easily assigned on the basis of charge concentration arguments only. In the example we reported, Co$_2$(CO)$_6$(AsPh$_3$)$_2$,[16] there are two kinds of bond between heavy atoms, Co−Co and Co−As, both having $\nabla^2\rho(r_b) > 0$ and small $\rho(r_b)$ like in closed shell interactions, although the former is expected to behave as an homopolar covalent bond and the latter as a donor−acceptor bond. It was suggested[16] that when at least one heavy atom is concerned, the radial shape of the atomic Laplacian makes the character of the interaction less clearly defined, requiring the inspection of other critical parameters for a better classification. At the critical point, covalent interactions are characterized by local excess of potential energy density ($V(r)$, everywhere negative) over the kinetic energy density ($G(r)$, everywhere positive). Thus the total energy density, $H(r) = G(r) + V(r)$, is negative at the *bcp*, and the ratio $G(r_b)/\rho(r_b)$ is small. Indeed, these features are found in M−M bonds whenever a direct bond path is observed (see Table 3). A similar reasoning was proposed by Molina et al. for Ga−Ga bond.[52] On the other hand, closed-shell interactions have a dominant $G(r_b)$,[53] which makes $G(r_b)/\rho(r_b)$ quite large and $H(r_b)$ positive.

Here, we will address the same problem with some additional tool. We have performed calculations on prototype molecules to test some bonding indicators such as the delocalization index

(49) Coppens, P.; Becker, P. J. *International Tables for Crystallography*, **1995**, *Vol. C*, 628.

(50) A chemical bond is associated with a line of maximum electron density, called the *bond path* (*bp*), which connects two bonded atoms. The atoms are characterised as maxima of $\rho(r)$ and are defined in space by an atomic basin. A saddle point of $\rho(r)$ along the bond path is called the *bond critical point* (*bcp*, **r$_b$**).

(51) Actually, in the experimental density a small ripple, identified as a maximum of $-\nabla^2\rho(r)$ is found also in the direction of Fe; however, it seems a very subtle feature, occurring at a much lower value of $|\nabla^2\rho(r)|$ and probably due to some ambiguity of the model. It is notable that this VSCC is not found in the theoretical density. In addition, the two distributions (experimental and theoretically) show a roughly similar shape of the (unique) envelope surrounding C(1), in contrast with the typical $\nabla^2\rho(r)$ picture of an organic $sp^2$ carbonyl (R$_2$C=O), characterised by two separated regions for the two C−R bonds. Another difference is the absence around C(1) of a VSCC pointing toward O(1) in the theoretical density. In fact, as it occurs also for free CO, the valence around the C atom is so polarised along the bond that a bonded VSCC is missing. On the contrary, the radial functions used for the experimental densities typically give rise to a shallow maximum of $-\nabla^2\rho(r)$ (see also ref 16).

(52) Molina-Molina, J.; Dobado, J. A.; Heard, L.; Bader, R. F. W.; Sundberg, M. R. *Ther. Chem. Acc.* **2001**, *105*, 365−373.

(53) Excess of kinetic energy density is related to Pauli repulsion between two closed shells, as it occurs for example on the interatomic surface separating two noble gases or ions. A useful way to put this index on an "absolute footing" is quantifying the kinetic energy per electron, $G(r_{bcp})/\rho(r_{bcp})$, which in general is in excess of unity for closed-shell interactions and in defect of unity for covalent bonds. However, $G(r_{bcp})/\rho(r_{bcp})$ increases as the interatomic surface lies closer to an atomic core, thus it grows with the bond order in homopolar interactions due to the smaller inter-nuclear separations (see for example the series C−C, C=C, and C≡C in Table 3) and in polar interactions because the interatomic surface is particularly penetrated into the atomic core of the electropositive atom.

**Chart 2**
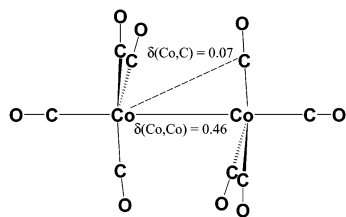


$\delta$ by Bader and Stephen[54] and the Mayer bond order[55] together with the usual QTAM parameters, including the electron density integrated on the interatomic surface, $\oint_{A \cap B} \rho(\mathbf{r})$, which is more informative than the simple electron density evaluated at the *bcp*. The analysis of Table 3 shows the typical features of homopolar covalent, heteropolar, ionic, and closed-shell noble gas bonds. We note that, on descending the periodic table, open-shell homopolar interactions (like Na−Na and K−K bonds in Na₂ and $K_2$ gas-phase molecules[56]) drastically decrease the electron density at the bond-critical point, but they do preserve a bond order of ca. 1, and the number of electron pairs shared by the two atoms (measured by $\delta$) also remains close 1.0, in agreement with the expectations of Lewis theory.[54b] The very diffuse character of their *s*-electrons, those mostly involved in the bonding of alkaline metal dimers, is responsible for the small electron density and the small and almost positive Laplacian observed in the region of the bonding (see the parameters computed at the *bcp*'s or integrated on the interatomic surface). The comparison with H₂ reveals the features that are instead preserved (and definitely different from those of noble-gas molecules): bond orders, $\delta$, $G(r_b)/\rho(r_b)$ and the sign of $H(r_b)$. On the other hand, $\rho(r_b)$, $\nabla^2\rho(r_b)$, $\oint_{A \cap B}\rho(\mathbf{r})$ and $|H(r_b)/\rho(r_b)|$ are more sensitive to the strength of the interaction and to the diffuse/contracted character of the orbitals involved in the bonding. Thus, it is not surprising that in an unsupported transition metal dimers (like $Co_2(CO)_8$ in $D_{3d}$ conformation), the M−M bond is characterized by a fairly larger electron density compared to Na₂ or $K_2$, either at the *bcp* or on the whole interatomic surface. In fact, the *s* orbital of a transition metal is more contracted than that of a same period alkaline metal, and a small *d*-orbital contribution may also occur. What is surprising instead is that the bond order and the number of electron pair shared is significantly smaller than 1.0. This is due to weak 1,3 interactions, which occur between a metal and all the vicinal carbonyls (especially the six in equatorial position, hereafter called *proximal* carbonyls), despite no 1,3 Co- - -C bond path is present (see Chart 2). Thus, the electrons are shared between the two metals and (partially) between each metal and all its *proximal* carbonyls. In fact, if we sum all these contribution

we recover the electron pair formally associated to a single M−M bond.

Noteworthy, the presence of such 1,3 interactions invalidate the framework of a fully localized 2c2e metal−metal bond, even for an unsupported dimer. We can say, instead, that the M−M electron sharing is the main interaction linking the two parts of the molecules when the M−C bonds are almost completely localized (i.e., in the absence of bridging or semibridging bonds). The comparison with $K_2$ or Na₂ molecules is particularly relevant for this conclusion. The more contracted nature of transition metal *s*-orbitals and the possible (though limited) *d*-orbital contribution produces more electron density for the metal−metal interaction, but the presence of ($\pi$-acidic) ligands around the dimer makes the bond order smaller.

These considerations can be used to characterize also the metal−ligand interactions reported in Table 2. The features of terminal M−C and C−O bonds of $[FeCo(CO)_8]^-$ conform to previous observations.[16,18] The electron density at the M−C *bcp* is relatively large (ca. 0.9 eÅ$^{-3}$), the $\nabla^2\rho(r_{bcp})$ is positive and the $H(r_{bcp})/\rho(r_{bcp})$ ratio is significantly negative (speaking for a relevant orbital contribution to the binding). The $G(r_{bcp})/\rho(r_{bcp})$ ratio is always quite large, reflecting the large Pauli repulsion term, as predicted by energy breakdown of M − $(CO)_n$ interactions.[53,57] The semibridging Co−C(1) bond shows the expected weakening, caused by the slight elongation. Although being the weakest metal−ligand bond, Fe−C(1) has more electron density than a typical single M−M bond (ca. 0.2 eÅ$^{-3}$),[16] and this could explain the Fe−Co bond path absence. The semibridging carbonyl is characterized by smaller density along the C−O path and a further shift of the *bcp* away from C, thus resulting in a less positive Laplacian compared to terminal CO.

Detecting the $\pi$-back-donation from the electron density distribution in metal carbonyl complexes is quite difficult because the pseudo-cylindrical symmetry of the density along the M−C bond paths cleans out traces of preferential accumulation planes (which anyway could be produced also by $\sigma$-donation). Moreover, atomic charges are sensitive to many different effects, like the polarity of the M−C bonds, and therefore, density accumulation on a CO ligand cannot be straightforwardly taken as an indicator of back-donation (though it can be useful for comparative purposes). The most reasonable sign of the back-bonding mechanism comes from the M- - -O delocalization index, $\delta(M,O)$. In fact, $\sigma$-donation involves mainly the metal and the carbon atoms. On the contrary, $\pi$-back-bonding must include a significant M- - -O sharing. For a terminal carbonyl in a neutral complex, $\delta(M,O)$ is about 0.15,[44] but it increases with the negative charge of the molecule. In $[FeCo(CO)_8]^-$, the terminal carbonyls have, on average, $\delta(Fe,O) = 0.20$ and $\delta(Co,O) = 0.18$. Noteworthy, for the semibridging carbonyl $\delta(Co,O) = 0.18$ and $\delta(Fe,O) = 0.09$, which means that the Fe−(CO) back-bonding is already quite significant, despite the long metal−carbonyl distance. This also agrees with the computed charge of the semibridging carbonyl ($Q = -0.40$), which is more negative than that of terminal COs ($Q = -0.25$). According to the above considerations, bridging carbonyls are more $\pi$-acidic than terminal ones. For example, in the sym-

(54) (a) Bader, R. F. W.; Stephens, M. E. *J. Am. Chem. Soc.* **1975**, *97*, 7391−7399. Through a partitioning of the pair density distribution a *localisation index* (number of electron pairs localised inside an atomic basin) and a *delocalisation index* (number of electron pairs delocalised between two atoms, hereafter $\delta(A, B)$) are defined. At the HF level of theory, $\delta(A, B)$ are in almost exact agreement with the Lewis theory, whereas post-HF correlated calculations show some significant reduction of the bonded electron pairs compared to the expectations of electron counting rules ((b) Fradera, X.; Austen, M. A.; Bader R. F. W. *J. Phys. Chem. A* **1999**, *103*, 304−314). By its definition $\delta(A, B)$ is not restricted to atoms sharing a common interatomic surface and therefore is an indicator able to depict the "electronic communication" between atoms.

(55) Mayer, I. *Chem. Phys. Lett.* **1983**, *97*, 270−274; Mayer, I. *Int. J. Quantum Chem.* **1984**, *26*, 151−154.

(56) Li−Li bond is excluded here because the density is characterised by nonnuclear maximum in the middle of the bond (Gatti, C.; Fantucci, P.; Pacchioni, G.; *Theor. Chim. Acta (Berlin)* **1987**, *72*, 433−458).

(57) Davidson, E. R.; Kunze, K. L.; Machado, F. B. C.; Chakravorty, S. J. *Acc. Chem. Res.* **1993**, *26*, 628−635.
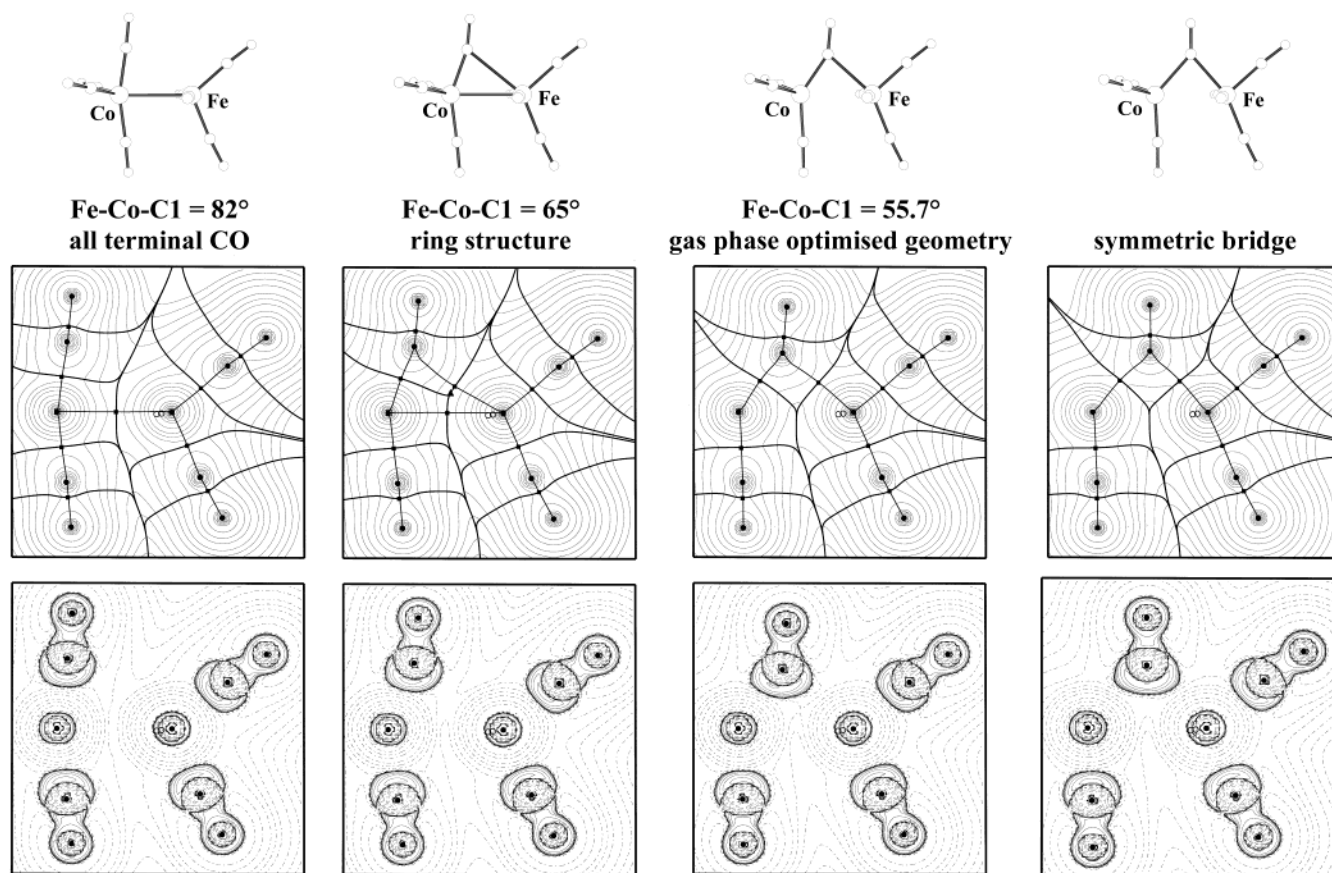
**Figure 3.** Geometrical features of the [FeCo(CO)$_8$]$^-$ anion along the conversion path from terminal to bridging (top); evolution of the electron density distribution, molecular graph and interatomic surfaces (center); evolution of the Laplacian distribution (bottom). For sake of simplicity, the geometry of the molecule was fixed on the gas-phase optimization but for the "bridging" carbonyl.

metrically bridged Co$_2$(CO)$_8$ ($C_{2v}$ isomer), $\delta$(Co1,O$_{bridging}$) + $\delta$(Co2,O$_{bridging}$) ∼2 $\delta$(M,O$_{terminal}$).[44]

**Terminal-to-Bridging Metamorphosis.** The experimental determination of the accurate electron density of [FeCo(CO)$_8$] [N(PPh$_3$)$_2$], [Co$_2$(CO)$_6$(AsPh$_3$)$_2$],[16] and [Co$_4$(CO)$_{11}$(PPh$_3$)][18] allows to draw the correlation like plot of Figure 4 which shows the early disappearance of the M−M bond path as a carbonyl starts to bridge a nearby metal. Of course, this observation is just based on three experimental determinations, and it cannot be considered fully representative of the evolution from terminal to bridging. To validate the correlation plot, we can focus on some theoretical investigations. Many transition-metal dimers have more than one stable isomer, as characterized by spectroscopic methods in solution or by gas-phase theoretical exploration of the potential energy surface. A notable example is Co$_2$(CO)$_8$, which has three minima corresponding to the only three kinds of isomers observed for the [M$_2$(CO)$_8$]$^{q-}$ species[58,59] (see Table 4), where coordinations **I**, **II**, and **III** are all recognizable. Their relative stability severely depends on the functional and the basis set (in agreement with what was found by Schaefer[58]); anyway, the energy window is quite small, giving an easy explanation for the observed fluxionality. However, only the (doubly bridged) $C_{2v}$ structure has been observed in the solid state.[60] Instead, the dianionic [Fe$_2$(CO)$_8$]$^{2-}$

(58) Kenny, J. P.; King, R. B.; Schaefer, H. F. *Inorg. Chem.* **2001**, *40*, 900−911.
(59) Aullón, G.; Alvarez, S. *Eur. J. Inorg. Chem.* **2001**, 3031−3038.
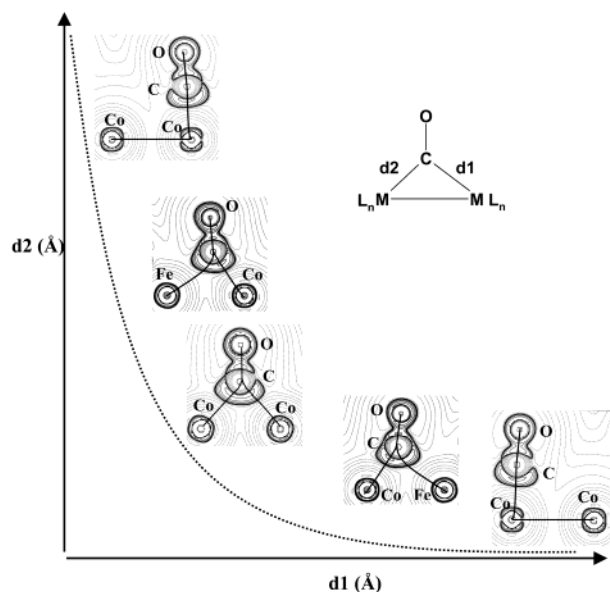(60) Leung, P. C.; Coppens, P. *Acta Crystallogr.* **1983**, *B39*, 535−542.

**Figure 4.** Same conformational space of the correlation plot of Figure 1 is here presented with $\nabla^2\rho(r)$ distribution of unsupported, semibridged and symmetrically bridged M−M interactions, from the accurate electron density determinations of Co$_2$(CO)$_6$(AsPPh$_3$)$_2$,[16] [FeCo(CO)$_8$][PPN] (this work), and Co$_4$(CO)$_{11}$PPh$_3$.[18] Note that the pictures have different features in the inner valence shell of the Co atoms compared to those of the original publications, due to some correction applied to the XD code.[28]

has only two gas-phase isomers, $D_{2d}$ and $D_{3d}$, the latter only being observed in the solid state.[61] The same two isomers are
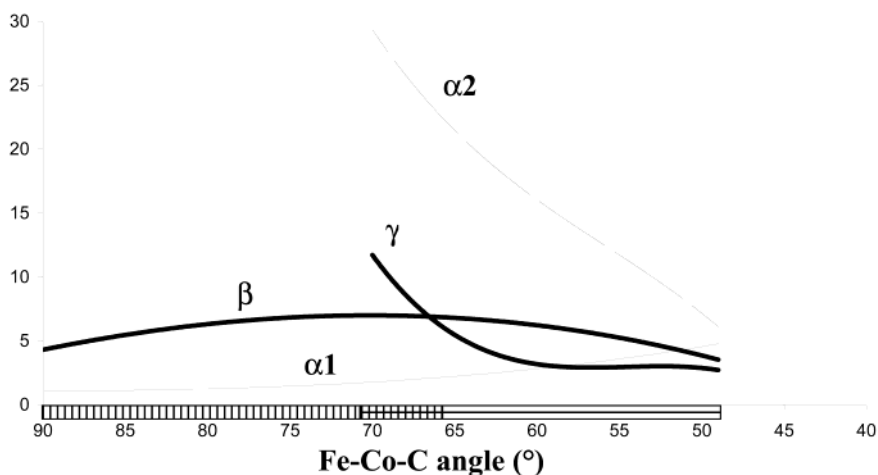
**Figure 5.** Evolution of the bond path angles (as defined in Chart 1) along the M-CO bending coordinate in $[FeCo(CO)_8]^-$.

theoretically predicted for $[FeCo(CO)_8]^-$ (lowered to $C_{3v}$ and $C_s$ symmetry, respectively), though only the $C_s$ form has been observed in the solid state so far. As can be concluded from Table 4, the molecular graph corresponding to coordination mode **I** is always characterized by a M−M bond path, whereas symmetric bridging coordination **III** invariably lacks of a bond path.[62] Instead, the semibridging mode **II** has a topology similar to **I** in $Co_2(CO)_8$ and $[Fe_2(CO)_8]^{2-}$ and similar to **III** in $[FeCo(CO)_8]^-$, where the semibridging character is more pronounced.

To better analyze the metamorphosis from a terminal to a bridging carbonyl, we have followed theoretically the evolution of $[FeCo(CO)_8]^-$ along the hypothetical path from a fully terminal (Fe−Co−C(1) > 80°) to a symmetrically bridged conformation (Fe−Co−C(1) = 49°) or, in other words, we have explored the neighborhood of the actual $C_s$ minimum (Fe−Co−C(1) = 55.7°) on the potential energy surface. The main changes observed in the electron density distribution on varying the Fe−Co−C(1) angle (see Figure 3) are summarized in the following points.

**Molecular Graph**. For a fully terminal system, the molecular graph is characterized by the Fe−Co and the eight M−C bond paths, without any 1,3 Fe···C interaction. As we noted in a previous work on the electron density of unsupported dimers,[16] the *bp* linking the metal to a terminal carbonyl (here Co−C(1)) is slightly bent in the direction of the proximal metal (see the bond path angles $\alpha1$ and $\beta$ in Chart 1 and Figure 5). For Fe−Co−C(1) ≈ 70°, an Fe−C(1) bond path appears and the molecular graph is now characterized by an Fe−Co−C(1) ring. The ring critical point is initially very close to the Fe−C(1) *bp*, and afterward, it moves toward the Fe−Co bond path, which eventually disappears for Fe−Co−C(1) ≤ 65°. The Fe−C(1) bond path is extremely inwardly curved in the initial steps (see

the bond path angle $\alpha2$ in Figure 5) but this curvature decreases as the Fe−C(1) bond reinforces. It is also quite interesting to follow the evolution of bond path angles at the metals ($\beta$ and $\gamma$ in Figure 5). Both have an inward curvature and we can summarize the observations as follows:

angles at carbon ($\alpha1, \alpha2$) measure the relative C→M donation, the larger is the deviation from a straight path, the weaker is the contribution; thus, because $\alpha1 < \alpha2$ the donation to Co is larger than that to Fe until the system reaches a symmetrical arrangement (and $\alpha1 \approx \alpha2$).

angles at the metals ($\beta$, $\gamma$) reflect the M→C back-donation; because $\gamma$ is always small, back-donation must be quite significant even for incipient semibridging coordination (actually $\gamma < \beta$, as discussed below).

Assuming that distortions of the valence shell distribution equally affect the metals and the carbon, from $\beta + \gamma < \alpha1 + \alpha2$, we may tentatively conclude that (Fe,Co)→C back-donation overwhelms C→(Co,Fe) donation along the conversion path and it is definitely more important in the symmetric bridging mode **II**.

**Laplacian Distribution**. The envelope of negative Laplacian of $\rho(r)$ surrounding a terminal carbonyl carbon is similar to that of an uncoordinated CO, though slightly distorted toward the proximal metal. The distortion increases as the carbonyl bends and the envelop becomes definitely larger in the symmetric bridge conformation, preserving however a unique maximum (i.e., a VSCC), see Figures 3 and 6. Note that in the symmetric bridging conformer the carbon VSCC is still slightly oriented toward Co, probably because the $Co(CO)_3$ fragment is particularly electron poor in this conformation and therefore it produces a larger attraction on the CO dative density. The single nonbonded VSCC of the oxygen is initially bent opposed to the proximal metal, though along the conversion path it moves on the other side (i.e., toward the proximal metal). After the ring graph is broken, a second nonbonded VSCC appears and the two C−O−VSCC angles approach 130°, see Figure 6. The *inner*-VSCCs of the metals (i.e., those of the 3d shell) also undergo a substantial modification. In the hypothetical $C_{4v}$ symmetry (which is not associated to any conformational minimum, because it has 2 imaginary frequencies), both metals are surrounded by a cube of maxima of $-\nabla^2\rho(r)$ with the four ligands and the M−M bond approximately disposed on the lateral faces (and an empty face opposed to the M−M bond),

(61) (a) Petz, W.; Weller, F. *Z. Kristallogr.-New Crystal Structures* **1997**, *212*, 157−158. (b) Bhattacharyya, N. K.; Coffy, T. J.; Quintana, W.; Salupo, T. A.; Bricker, J. C.; Shay, T. B.; Payne, M.; Shore, S. G. *Organometallics* **1990**, *9*, 2368−2374. (c) Cassidy, J. M.; Whitmire, K. H.; Long G. J. *J. Organomet. Chem.* **1992**, *427*, 355−362. (d) Bockman, T. M.; Cho, H.-C.; Kochi, J. K. *Organometallics* **1995**, *14*, 5221−5231. (e) See also ref. 21. Recently, the $C_{2v}$ isomer (which is not a minimum in the gas phase) has been observed in the strong polarising environment produced by Li cations (Neumuller, B.; Petz, W. *Organometallics* **2001**, *20*, 163−170.

(62) In $[Fe_2(CO)_8]^{2-}$ and $[FeCo(CO)_8]^-$, the coordination **III** is not associated to a stable isomer, since the corresponding equilibrium geometries have at least one imaginary frequency. However, the theoretical observation that symmetric bridges quench the MM bond path is well supported in many analogous fragments.
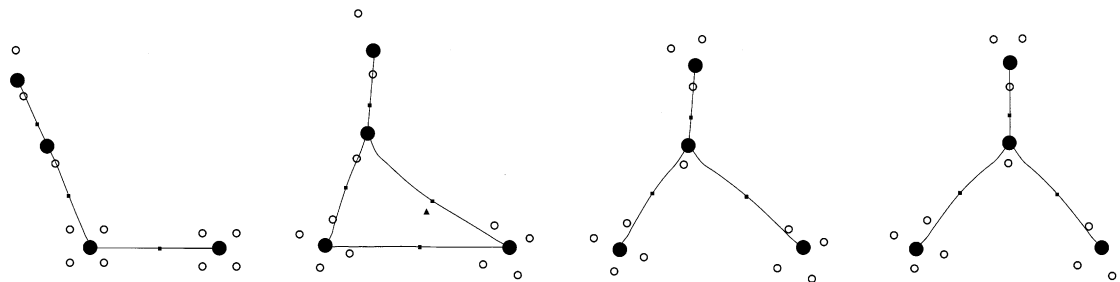
**Figure 6.** Evolution of the VSCCs around Fe, Co, C(1) and O(1) (here represented with white circles) along the M-CO bending coordinate. The bond paths, nuclear positions, and *bcp* of each molecular graph are represented.
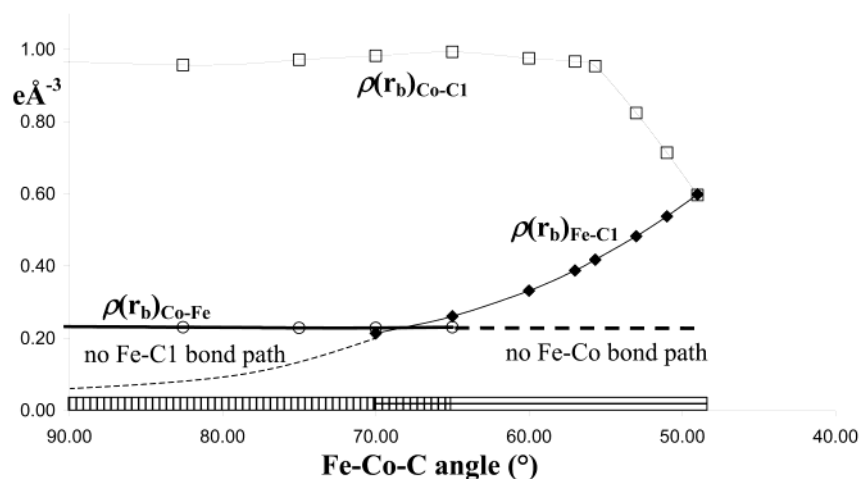


**Figure 7.** Evolution of the electron density computed at the *bcp* of the Fe−C(1), Fe−Co, and Co−C(1) interactions.

see Figure 6. When the terminal ligands are disposed in the same conformation adopted by the semibridging dimer, the cubes are distorted and rotated. After the bending of C(1), the polyhedron surrounding Co is again slightly rotated and eventually, one of the vertexes is lost. It is notable that the conformation adopted seems to favor the back-donation from Fe to C(1).

**Atomic Charges**. According to different partitioning schemes, before the bending of the semibridging CO the negative charge is mostly localized in the Fe(CO)$_4$ moiety ($Q = -0.59$).[63] At the equilibrium geometry the two parts of the molecule have an almost identical QTAM charge, with $Q[\text{Fe(CO)}_4] = -0.48$, and eventually $Q[\text{Fe(CO)}_4] = -0.15$ in the symmetric bridge conformation. The charge equalization occurring in the semibridging conformation is confirmed by the experimental monopoles, $Q[\text{Fe(CO)}_4] = -0.48$, and it is in agreement with the metal−carbonyl bond distances observed, which speak for an intermediate charge on both fragments. It is also notable that the charge accumulation on the semibridging carbonyl increases upon bending, in agreement with the increased back-donation, as revealed by other parameters described above.

**Bond Indexes**. The main changes occurring can be summarized as follows:

$\rho(r_b)_{\text{Fe−Co}}$ is quite constant until the bond path breaks; when the ring is formed, $\rho(r_b)_{\text{Fe−C}} < \rho(r_b)_{\text{Fe−Co}}$, but it rapidly increases up to the value of a symmetric bridging coordination, where $\rho(r_b)_{\text{Fe−C}} \approx \rho(r_b)_{\text{Co−C}}$ (anyway larger than one-half $\rho(r_b)$ of a terminal M-CO), see Figure 7.

---

(63) This charge is obtained by integrating the electron density over the atomic basins of the Fe(CO)$_4$ moiety.

The three corresponding $\oint_{A\cap B}\rho(\mathbf{r})$ show similar evolutions, though with a more pronounced decrease for Fe−Co density, see Figure 8.

$\delta(\text{Fe−Co})$ smoothly decays, whereas $\delta(\text{Fe−C(1)})$ more rapidly grows; all the other metal-proximal carbonyl delocalization indexes remain constant. Overall, the summation of the delocalization indexes involving the two metals and the bending carbonyl is almost constant to 2.0 electron pairs, see Figure 9.

The Mayer bond orders do behave in a very similar way: in the terminal coordination mode the Co−Fe bond order is 0.47, and it decreases to 0.39; the 1,3 Fe- - -C bond order is 0.08, and it grows to 0.48 in the semibridging conformation

According to these and the above observations, the [Co(CO)$_3$], [(CO)], and [Fe(CO)$_4$]$^-$ fragments are held together, along the *whole* reaction path, by four electrons distributed over three major interactions (Fe−Co, Fe−C(1), Co−C(1)) and many small, thought not negligible, metal-proximal carbonyl interactions. The latter are mainly responsible of the small M−M bond orders in transition metal carbonyl clusters but they do not substantially affect the evolution of the molecular graph shape along the conversion path. Instead, it is the relative amount of the three main components, strongly dependent on the Fe−Co−C angle, which eventually determines the abrupt changes in the molecular graph shape. In particular, the M−M bond path disappears as soon as the Fe−C contribution overwhelms the Fe−Co one, as measured either by $\delta$ or by $\rho(r_b)$.

Another interesting feature revealed by this analysis is that Fe−C(1) bond is mainly due to metal back-donation (as in Chart 3). In fact, the Fe−C(1) *bp* is extremely distorted at C(1), where donation is dominant. In addition, the disposition of metal *inner-*
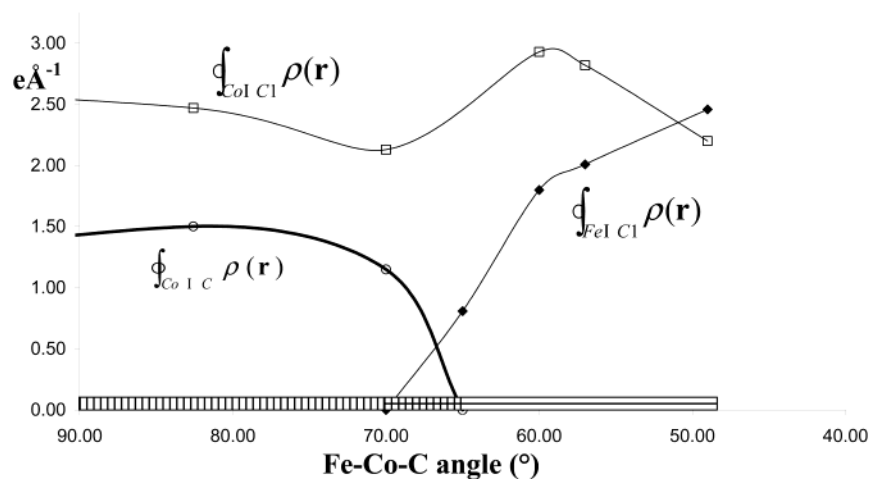
**Figure 8.** Evolution of the electron density integrated over the interatomic surface of the Fe−C(1), Fe−Co, and Co−C(1) interactions.
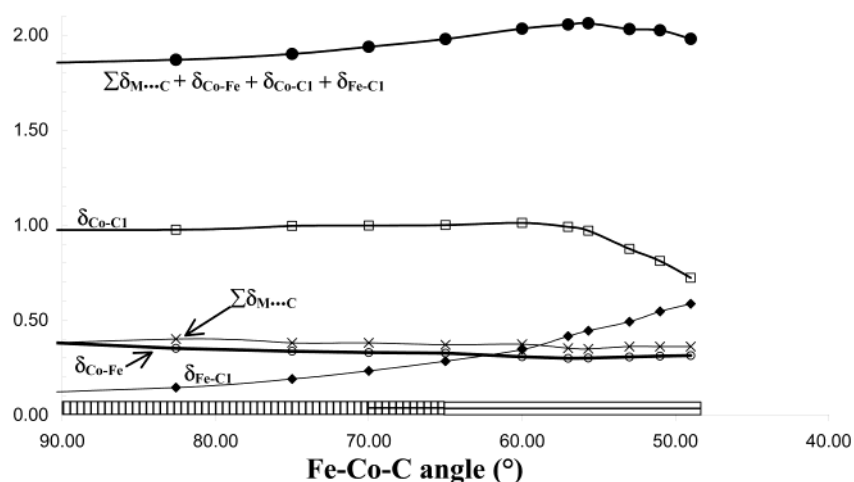


**Figure 9.** Evolution of the delocalization indexes of the Co−Fe, Co−C(1), Fe−C(1), and 1,3 M- - -C interactions.

VSCCs and carbonyl VSCC do suggest an unfavorable situation for the donation mechanism, and the large $\delta(Fe,O)$ delocalization is consistent with considerable back-donation. We may conclude that along the terminal-to-bridging conversion, back-donation is "activated" earlier and eventually the M→C electron flow overcomes the C→M one even in symmetric bridge, as revealed by the larger negative charges and C−O distances of bridging carbonyls.

**Through Bond vs Through Space Interactions?** According to bond indexes, there is a continuum between terminal and bridging carbonyls, provided that we take into account the mutual interplay of M−M, M···M, M−C, and M···C interactions. It is however difficult, to find a conceptual frame, within QTAM, for the 1,3 M- - -C and M···M interactions when their bond paths lack.

From an 'orbital interaction' point of view, one could be tempted to associate the presence of a bond path to a direct *through space* coupling of atomic orbitals and the significant delocalization between two atoms not connected by a bond path to a *through bond* coupling mechanism.[64] However, all orbitals, molecular and basis functions, extend over the complete molecule and distant atoms "talk" to one another through the mechanism of exchange (as measured by $\delta$). Thus, to ascertain

**Chart 3**
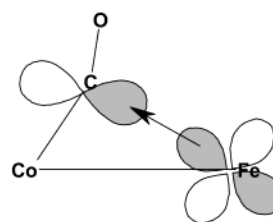


or exclude a *significant* direct coupling is always rather arbitrary.[65]

Alternatively, from a "valence bond" point of view, we may think that different "resonant" spin-pairing structures (the M−C's and the M−M) contribute to the delocalized bonding in the given 'molecule' and to the pertinent delocalization indexes as the degree of pairing.

In both cases, we may assume that whenever two direct interactions compete, the strongest will always give rise to a

(64) Hoffmann, R. *Acc. Chem. Res.* **1971**, *4*, 1−9.

(65) Support to the significant *through bond* nature of the 1,3 M- - -C interaction comes from the analysis of the $D_{3d}$ conformation of $Co_2(CO)_8$, where 1,3 Co- - -C delocalisation is found even with the axial carbonyls. Given the relatively large distortion of the bond path at Co (see angle $\beta$) even for those conformations where a direct Fe−C(1) is absent, the Co−C(1) interaction could be carrier of the *through bond* mechanism. In fact, the observed $\beta > \alpha1$ and $\beta > \gamma$ are justified only if we consider a "CO-insertion" into the M−M direct coupling (a direct Fe−C(1) coupling would not affect $\beta$).

bond path, while the weakest could be canceled. In this view, the long range 1,3 M- - -C interaction would be definitely weak compared to M−M bond in unsupported dimers as well as the M- - -M interaction (compared to M−C−M) in bridged dimers.

Recent theoretical calculations on [CpNi($\mu_2$-InMe)$_2$NiCp][66] (the InMe group being isolobal to CO)[67] report the presence a direct M−M bond path (and a cyclic molecular graph). A similar topology was observed in the experimental analysis[68] of (CO)$_3$-Co($\mu_2$−CO)($\mu_2$−C$_4$O$_2$H$_2$)Co(CO)$_3$, where both a carbonyl and an oxofuranic group bridge the Co−Co edge. Both derivatives are "isoelectronic" and structurally related to the $C_{2v}$ isomer of Co$_2$(CO)$_8$ but their geometry are somewhat 'distorted' with respect to that of the 'parent' compound. In CpNi($\mu_2$−InCH$_3$)$_2$-NiCp, the $\mu_2$−InCH$_3$ ligand has a significantly weaker interaction than $\mu_2$−CO, accordingly it lies much further from the metals. On the other hand, $\mu_2$−C$_4$O$_2$H$_2$ in Co$_2$(CO)$_6$($\mu_2$−CO)-($\mu_2$-C$_4$O$_2$H$_2$) induces a compression of the Co−Co distance, which is 0.1 Å shorter than in Co$_2$(CO)$_8$. The fact that both a stretching of the bridging ligand and a compression of the metal−metal bond produce a ring structure with a direct M−M bond path, extends the bonding picture drawn above to a wider part of conformational space. Although preliminary theoretical calculations[44] on Co$_2$(CO)$_6$($\mu_2$−CO)($\mu_2$−C$_4$O$_2$H$_2$) do not confirm the experimental topology reported,[68] exploration of the potential energy surface of a symmetrical single-bridged dimer, namely Ni$_2$(CO)$_7$,[44] shows that the two deformations from the equilibrium geometry (which lacks of a MM bond path) do in fact produce a molecular graph characterized by a ring. Thus, the stability of the cyclic graph is somewhat wider if coordinates other than the M−M−C angle are considered.

## Conclusions

In this work, we have determined (experimentally) the accurate electron density of the [FeCo(CO)$_8$][N(PPh$_3$)$_2$] salt by low-temperature X-ray diffraction and monitored (theoretically) the gas-phase transformation of the [FeCo(CO)$_8$]$^-$ semi-bridging carbonyl, into a symmetric bridging or a terminal one. This has allowed to recognize the mutual interplay of M−M, M−C, M- - -M, and M- - -C interactions along the conversion path, to reach a unitary picture for both supported and unsupported metal−metal interactions and to shed some light on the broad region of the conformational space of metal carbonyl clusters associated with the presence of a semi-bridging ligand.

Despite the typical weakness of interactions between open shell metals, unsupported metal−metal bonds show some features of genuine covalent bonds: the total electron density shared on the interatomic surface may be as large as in many undisputed single bonds; the number of shared electron pairs is close to 1.0 (or more generally to the expected formal bond order), unless *some* three-center bonding with one or more (acidic) ligand groups occurs; the energy density at the bond critical point is small but negative, indicating a dominant contribution of the potential energy. The small amount of electron density at the bond critical point and its corresponding positive Laplacian are due to the very diffuse character of the *ns* valence electrons of the metal atoms, evidenced by the lack of outermost charge concentration even in the isolated metal atoms.

On the other hand, $\mu_2$-carbonyl ligands bind the metals through delocalized 3c−4e bonds. No bond path directly linking the two metal is normally observed, despite the M−M distances are shorter than their unsupported counterparts. The two M−C bond paths are curved in the direction of the absent M−M edge, speaking for a "concerted" mechanism. $\mu_2$-carbonyl ligands show large[69] *sp*-like VSCC distributions at variance from organic R$_2$C=O carbonyls, which have *sp*$^2$-like VSCC distributions and localized 2c−2e R−C bonds. Bridging carbonyls require more metal orbitals than terminal COs, thus they compete with the direct metal−metal interactions, as manifested by the delocalization indexes $\delta$ and Mayer's bond orders. Even the weaker semibridging carbonyl annihilates the subtended M−M bond path by affording an (asymmetric) three-center bond, in fact the metal−metal bond path disappears quite early along the evolution coordinate. The semibridging coordination seems to realize the most efficient charge transfer from the electron rich part of the system to the electron poor one.

Analyzing the solid state conformation of transition metal dimers, a continuum of coordination mode from terminal to symmetric $\mu_2$−CO is observed, despite the abrupt change of the molecular graph structure (hence of the bond description). The different isomers of a M$_2$(CO)$_n$ system may be simply regarded as produced by slightly different "weightings" of the M−M and M−C interactions, well described by the corresponding delocalization indexes without any definitive breakdown. This view rationalizes the usually small energy separation between conformers, the fluxionality of metal clusters, the substantial continuity of the observed solid state conformations. It is notable that although "traditional" bonding schemes may be less powerful in revealing this framework, through the analysis of the electron density distribution we can confine the three isomers in the conformational space and, at the same time, assess their weak structural stability.

It is important stressing that a given molecular graph cannot be straightforwardly regarded in terms of classical MO schemes because a bond path does not contain itself information on the actual number of electrons shared by the two linked atoms (0, 2, 4 etc.) nor can it give information on the occurrence of some delocalized bonding. Within the QTAM approach, this information is actually contained in the delocalization indexes $\delta$ (and indirectly in the shape of the bond path if a nonlinear molecule is concerned). The framework here presented goes beyond a classical view of transition metal dimers giving a more flexible representation of the bonding, in agreement with the experimental observations reported.

**Supporting Information Available:** Figures: experimental deformation density (S1a, S1c) and residual density (S1b, S1d) in the Fe−Co−C(1) plane and in a phenyl ring of the cation; ORTEP view with complete labeling scheme of the anion (S2). Tables: geometrical parameters from the RT (S1, S3) and 125 K (S2, S4) experiments; multipolar parameters refined (S5). This material is available free of charge via the Internet at http://pubs.acs.org.

JA026186E

(66) Uhl, W.; Melle, S.; Frenking, G.; Hartmann, M. *Inorg. Chem.* **2001**, *40*, 750−755.
(67) Uhl, W.; Pohlmann, M.; Wartchow, R. *Angew. Chem., Int. Ed.* **1998**, *37*, 961−963.
(68) Bianchi, R.; Gervasio, G.; Marabello, D. *Helv. Chim. Acta.* **2001**, *84*, 722−734.

(69) Larger than those of terminal carbonyls and free CO.
(70) Abramov, Y. A. *Acta Crystallogr.* **1997**, *A53*, 264−272.